(DOI will not work until issue is live.) DOI: http://dx.doi.org/10.2138/am-2015-5022

Revision 1

Direct observation of Ca-Na ordering and structure polarity in Ca-rich intermediate plagioclase feldspar with incommensurate modulated structure

Huifang Xu

NASA Astrobiology Institute, Department of Geoscience and Materials Science Program

University of Wisconsin-Madison

1215 W Dayton St., Madison, WI 53706, USA

* Corresponding author: Dr. Huifang Xu

Tel: 1-608-265-5887

Fax: 1-608-262-0693

Email: hfxu@geology.wisc.edu

Abstract

Ca-Na ordering and structural polarity of subcells in an intermediate plagioclase with modulated structure have been observed using Z-contrast imaging methodology with an aberration-corrected scanning transmission electron microscope. Neighboring lamellar domains with $I1$ symmetry are related by inversion twin operation, instead of anti-phase domain boundaries (or, APBs) as in all previously reported structure models. The boundaries between lamellar domains have $I\bar{1}$ symmetry instead of $C\bar{1}$ symmetry. Modulated plagioclase has unique Ca-Na and Al-Si ordering structure that is different from those in end-member structures of anorthite and low albite. The modulated structures of intermediate plagioclase are not metastable structures formed during phase transition, but rather thermodynamically stable structures at low temperature due to Ca-Na ordering within the subcells with $I1$ symmetry.

Introduction

Although plagioclase feldspars are the most abundant mineral in the earth's crust, their crystal structures and the formation mechanism of modulated structure in intermediate plagioclase have been an enigma for decades beginning with the first discovery of modulated structure in 1940 (Chao and Taylor, 1940; Kirkpatrick et al., 1987; McConnell, 2008; Smith and Brown, 1988). Low temperature intermediate plagioclase feldspars (An 25 – An75) display major *a*-reflections ($l=2n$, $h+k=2n$) and extra satellite reflections (*e*- and *f*- reflections) that characterize incommensurate modulated structures, or *e*-plagioclase (Ribbe, 1983; Smith and Brown, 1988). The *e*-reflections are pairs of satellite diffraction spots neighboring *b* reflections ($l=2n+1$, $h+k+l=2n$), although the *b*-reflections do not appear. The *f*-reflections are pairs of weak satellite diffraction spots neighboring *a*-reflections (Ribbe, 1983). Crystal structure models for modulated plagioclase still remain controversial. For example, multiple structure models have been proposed based on the exact same set of experimental data (Horst et al., 1981; Yamamoto, 1984). Modulated structure and its formation mechanism affect subsolidus phase relations in intermediate plagioclase feldspars (Carpenter, 1994; Grove et al., 1983; Smith and Brown, 1988). It is important to understand crystal structure of modulated structures in intermediate plagioclase. All proposed structure models based on X-ray diffraction and transmission electron microscopic studies can be categorized into two groups:

Periodic alternating lamellae with anorthite ($I\bar{1}$) structure in anti-phase relationship with a stacking vector of ½ ***c***, or ½ [***a+b***]: An…An*…An…. (McConnell, 1963; Horst et al., 1981; Wenk and Nakajima, 1980). The symbols An and An* represent plagioclase lamellar domains with anorthite-like structure in anti-phase relationship. The boundaries (APBs) will have $C\bar{1}$ symmetry.

Periodic alternating lamellae with anorthite ($I\bar{1}$) and albite ($C\bar{1}$) structures. Anorthite-like lamellae are in anti-phase relationship with albite-like domains at the boundary (i.e., anti-phase domain boundary or, APB) positions: An…Ab…An*…Ab…An… (Grove, 1977; Kumao et al., 1981; Nakajima et al., 1977; Smith and Ribbe, 1969; Yamamoto et al., 1982, 1984). This group of models displays density modulation (or compositional variation along the modulation direction) in addition to the anti-phase relationship.

All proposed models are based on anorthite and albite-like subunits. However, Al-Si ordering (like Al occupancy in T10 site) and electron density mapping of Ca-Na atoms indicate that the incommensurate modulated structure is not a mixture of low albite and anorthite subunits based on the average structure of modulated plagioclase feldspars studied to date (Kitamura et al., 1984; Ribbe, 1983; Smith and Brown, 1988; Wenk et al., 1980)..

Sample and Experimental Methods

The studied bytownite sample is from an anorthosite in Roosevelt, Kiowa County, Oklahoma. The composition of plagioclase ranges from ~An65 to ~An75 (Powell and Fischer, 1976). A plagioclase crystal with ~An70 was selected for Z-contrast imaging analyses. Composition of the crystal grain was analyzed using X-ray energy-dispersive spectroscopy (EDS) methodology after acquiring Z-contrast images. The k-factors for Na, Ca, and Al, which are required for quantitative EDS analyses of the plagioclase were determined using standards of albite and a synthetic anorthite. The crystal displays homogeneous modulated structure without any exsolution lamellae.

Scanning transmission electron microscopy (STEM) analyses were carried out using a FEI Titan 80-200 aberration-corrected STEM operated at 200 kV. The microscope is equipped with a CEOS probe aberration corrector, an EDAX high-resolution X-ray energy-dispersive (EDS) detector, and a Gatan image filtering system. All Z-contrast images were acquired using camera length of 160 mm in order to maximize differences among different atoms (Xu et al., 2014). The high-angle annular dark-field (HAADF) STEM imaging (or Z-contrast imaging) is capable of a spatial resolution <0.1 nm using aberration-corrected STEM. Signal intensity is proportional to atomic number (~Z^2) and number of atoms along the beam direction for the imaging acquisition condition (Kirkland, 1998; Pennycook, 2002). The TEM samples were prepared by crushing the selected bytownite grain between two glass slides with ethanol. A drop of the suspension was placed on a lacey-carbon Cu grid and air dried. The specimen was lightly plasma cleaned before insertion into the STEM column on a double-tilt specimen holder. Interesting areas and crystal grains with needed zone-axis orientations were located using TEM mode, due to the ease with which appropriate zone-axis orientation can be identified under TEM mode. The probe aberration correction was carried out first using a standard sample of nano-gold particles on a single-tilt specimen holder. The double-tilt specimen holder containing the bytownite specimen was again inserted into the STEM column for Z-contrast imaging under STEM mode. Switching from STEM mode to TEM mode will lose aberration-corrected conditions.

Results and Discussions

The selected area electron diffraction pattern from the bytownite (~An72) investigated here, displays strong *a*-reflections, weak *e*-reflections, and very weak *f*-reflections (Fig. 1A). No exsolution lamellae were observed in the studied sample, although it is within the Huttenlocher intergrowth region. Micro-exsolution lamellae in some bytownite samples occur only in rock that cooled extremely slow (Grove, 1976; Smith and Brown, 1988). A plagioclase grain with An72 was chosen for Z-contrast imaging because the modulation direction for ~An70 plagiolcase is very close to $(0\bar{1}1)^*$ direction, i.e., about normal to $(0\bar{1}1)$ (Ribbe, 1983; Smith and Brown, 1988). The modulation direction will be approximately perpendicular to the ***a***-axis, a main direction of feldspar. Z-contrast images along the ***a***-axis will reveal structure variation along the modulation direction clearly.

The obtained Z-contrast image along the ***a***-axis clearly shows ordering of Ca atoms (indicated by arrows) along ~ $(0\bar{1}1)$ planes (Fig. 2B). Signal intensity in Z-contrast images is directly related to atomic number (Z) and occupancy of the atoms (Pennycook, 2002). Z-contrast images are very sensitive to compositional change or variation. Z-contrast imaging that uses non-coherent electrons scattered at high angle can avoid multiple diffraction that occurs in high-resolution TEM imaging (Kirkland, 1998; Pennycook, 2002). No compositional or density modulation is observed in Z-contrast images collected during this study. Fast Fourier transform (FFT) patterns from Z-contrast images do not show satellite reflections around the 000 spot (Fig. 1C). If composition or density modulation occurs in the crystal, satellite reflections will occur around the 000 spot (Smith and Brown, 1988). The Ca-Na ordering phenomenon is obvious in a noise-filtered Z-contrast image (Fig. 3). Arrows indicate Ca ordering at the boundaries (~ // $(0\bar{1}1)$) between the lamellar domains (Fig. 3). Outlines of unit cells (based on body-centered setting of plagioclase) for the subcells are also inserted in the image. Yellow outlines are for subcells in the lamellar domains. Red outlines are for subcells at the boundaries between the neighboring

This is a preprint, the final version is subject to change, of the American Mineralogist (MSA)
Cite as Authors (Year) Title. American Mineralogist, in press.
(DOI will not work until issue is live.) DOI: http://dx.doi.org/10.2138/am-2015-5022

domains (Fig. 3). Based on the intensities of Ca-Na (or, M) sites in the lamellar domains, subcells do not have a symmetry center (or inversion center). Possible symmetry for the subcells in the lamellar domains is $I1$, instead of $I\bar{1}$. Neighboring lamellar domains with $I1$ symmetry are in an inversion twinning relationship. Structure models for the subcell domains and an inversion twin boundary between neighboring lamellar domains are proposed in Figure 4. Al-Si ordering structure in subcells with $I1$ symmetry is different from analogous ordering in low albite and anorthite. Structures of albite and anorthite along ***a***-axis are also illustrated in Fig. 5 (Angel, 1988; Harlow and Brown, 1980; Wainwright and Starkey, 1971). The subcell has an anorthite sub unit with anorthite-like Al-Si ordering (Fig. 4C, 4D). However, in the albite-like subunit, only one of the two T1o sites can be filled by Al. This follows the Al avoidance rule due to Al in the anorthite region. Remaining Al will be distributed in T1m, T2m, and T2o sites in the albite-like region (Fig. 4C, 4D). Al occupancy in the T1o site for the $I1$ structure (Figs. 4C, 4D) will be 0.5 using an average structure with $C\bar{1}$ symmetry. Al occupancies in T1o sites of the average $C\bar{1}$ symmetry structure will not be compatible with a mixture of low albite and anorthite subunits. This is consistent with the observed Al-Si ordering in average structure of modulated plagioclase feldspars (Figure 16 of Ribbe, 1972; Figure 3.8 of Smith and Brown, 1988). Proposed structure types with Ca-Na polarity in the modulated structure may explain unique electron density of M (Ca-Na) sites in average $C\bar{1}$ symmetry structures compared to a simple mixture of anorthite and low albite domains. The structure at the inversion boundary will have $I\bar{1}$ symmetry with Ca-Na ordering in 0 and z sites, respectively (Fig. 4B). Modulation in *e*-plagioclase is not a compositional or density modulation, but a positional modulation involving shifts and ordering of Ca-Na and Al-Si atoms within the subcells (Fig. 6).

Satellite reflections characterizing the modulated structure can also be observed in a $[\bar{1}\bar{1}\bar{1}]$-zone-axis diffraction pattern (Fig. 7A). A Z-contrast image and its noise-filtered image along the $[\bar{1}\bar{1}\bar{1}]$-zone-axis shows structural modulation along ~ $(0\bar{1}1)^*$ direction (Fig. 8A, 8B). The observed image also indicates that the subcells in the lamellar domains do not have an inversion center (Fig. 7D). Projection of the proposed *I*1 symmetry structure along $[\bar{1}\bar{1}\bar{1}]$ direction (Fig. 8C) matches evidence presented in the image (Fig. 8D). Periodic big dark (labeled "D") and small less dark (labeled "LD") areas along ***c***-axis result from Ca-Na ordering in the subcells of a lamellar domain (Fig. 8D). If the subcells have inversion operation, the features of dark areas should be the same because they are related by an inversion center.

Toman and Frueh (1976) proposed periodic APBs for modulated structure if subcells are centric. They also proposed the possibility of a periodic inversion boundary for modulated structure if subcells are non-centric (Toman and Frueh, 1976). However, X-ray diffraction alone cannot tell the difference between the two possibilities (Toman and Frueh, 1976). As an alternative, McConnell (2008) proposed a Ca-Na ordered structure for subcells with a primitive Bravais lattice in the modulated structure. In this case the proposed periodic anti-phase lamellae domains are related by a translational vector of ½ [**a**+**b**+**c**] (McConnell, 2008). This is not consistent with the observed Z-contrast images presented here.

Implications

The transition of An-rich plagioclase from $I\bar{1}$ to *I*1 symmetry involves slight changes in Al-Si ordering structure, i.e., movement of residual Al in some Si sites (blue) to neighboring Al sites

(Fig. 4B). Ca-Na ordering will result in Al ordering around Ca atom pairs (Figs. 4C, 4D). Phase transition from $I\bar{1}$ to the modulated structure is a Na-Ca ordering process accompanied by Al-Si ordering within the subcells with $I1$ symmetry. The neighboring lamellar domains of $I1$ symmetry are related by inversion twin operation. The newly discovered structure for the intermediate plagioclase helps to understand Al-Si ordering and the subsolidus phase diagram of plagioclase. Ca-Na ordering in intermediate plagioclase may lower the total energy and stabilize the modulated structure (McConnell, 2008). The observed enthalpy difference between ordered and disordered labradorite may support Ca-Na ordering in addition to the Al-Si ordering (Carpenter et al., 1985).

ACKNOWLEDGEMENTS

This work is supported by NSF (EAR-095800, EAR-0810150, and DMR-0619368, MRI) and NASA Astrobiology Institute (N07-5489). The author thanks Dr. Hiromi Konishi for helping with image acquisition, Dr. Alex Kivit for optimizing the microscope, and Zhizhang Shen and Nick Levitt for insightful discussions and suggestions. The author also thanks Prof. Michael Carpenter and an anonymous reviewer for their comments.

References

Angel, R.J. (1988) High-pressure structure of anorthite Sample: P = 31 kbar. American Mineralogist, 73, 1114-1119.

Carpenter, M.A. (1994) Subsolidus phase relations of the plagioclase feldspar solid solution, in: Parsons, I. (Ed.), Feldspars and their reactions. Kluwer Academic Publishers, Dordrecht, pp. 221-269.

Carpenter, M.A., McConnell, J.D.C., and Navrotsky, A. (1985) Enthalpies of ordering in the plagioclase feldspar solid-solution. Geochimica et Cosmochimica Acta, 49, 947-966.

Chao, S.H., Taylor, and W.H. (1940) Isomorphous replacement and superlattice structures in the plagioclase feldspars. Proceedings of Royal Society (London), 176A, 76-87.

Grove, T.L. (1976) Exsolution in metamorphic byrownite. In H.-R. Wen ked. “Electron Microscopy in Mineralogy”. Springer-Verlag, Berlin, pp. 266-270.

Grove, T.L. (1977) Periodic antiphase structure model for intermediate plagioclases (An33 to An75). American Mineralogist, 62, 932-941.

Grove, T.L., Ferry, J.M., and Spear, F.S. (1983) Phase-transitions and decomposition relations in calcic plagioclase. American Mineralogist, 68, 41-59.

Harlow, G.E., and Brown, G.E. (1980) Low albite: an X-ray and neutron diffraction study. American Mineralogist, 65, 986-995.

Horst, W., Tagai, T., Korekawa, M., and Jagodzinski, H. (1981) Modulated structure of a plagioclase-An52 - theory and structure determination. Zeitschrift Fur Kristallographie, 157, 233-250.

Kirkland, E.J., 1998. Advanced computing in electron microscopy. Plenum Press New York.

Kirkpatrick, R.J., Carpenter, M.A., Yang, W.H., and Montez, B. (1987) Si-29 magic-angle nmr-spectroscopy of low-temperature ordered plagioclase feldspars. Nature, 325, 236-238.

Kitamura, M., Morimoto, N., Yamamoto, and A., Nakazawa, H. (1984) The modulated structure of the e-plagioclase feldspars. Acta Crystallographica, Section A 40, C251-C251.

Kumao, A., Hashimoto, H., Nissen, H.U., and Endoh, H. (1981) Ca and Na positions in labradorite feldspar as derived from high-resolution electron-microscopy and optical diffraction. Acta Crystallographica, Section A 37, 229-238.

McConnell, J.D.C., (1963) Direct electron-optical resolution of anti-phase domains in a silicate. Nature, 199, 586.

McConnell, J.D.C. (2008) The origin and characteristics of the incommensurate structures in the plagioclase feldspars. Canadian Mineralogist, 46, 1389-1400.

Nakajima, Y., Morimoto, N., and Kitamura, M. (1977) Superstructure of plagioclase feldspars - electron-microscopic study of anorthite and labradorite. Physics and Chemistry of Minerals, 1, 213-225.

Pennycook, S. (2002) Structure determination through Z-contrast microscopy. Advances in Imaging and Electron Physics, 123, 173-206.

Powell, B.N., and Fischer, J.F. (1976) Plutonic igneous geology of the wichita magmatic province, Oklahoma. Oklahoma Geological Survey, Norman.

Ribbe, P.H. (1972) One-parameter characterization of average Al/Si distribution in plagioclase feldspars. Journal of Geophysical Research, 77, 5790.

Ribbe, P.H. (1983) Aluminum-silicon order in feldspars: Domain textures and diffraction patterns, in: Ribbe, P.H. (Ed.), Rivews in Mineralogy, Vol. 2 Feldspar Mineralogy, 2 ed. Mineralogical Society of America, Washington, D. C., pp. 21-55.

Smith, J.V., and Brown, W.L. (1988) Feldspar minerals 1: crystal structures, physical, chemical and microtextural properties. Springer-Verlag, Berlin, Germany. pp. 31-117.

Smith, J.V., and Ribbe, P.H. (1969) Atomic movements in plagioclase feldspars - kinetic interpretation. Contributions to Mineralogy and Petrology, 21, 157-202.

Toman, K., and Frueh, A.J. (1976) Modulated structure of an intermediate plagioclase. 2. Numerical results and discussion. Acta Crystallographica, Section B 32, 526-538.

Wainwright, J.E., and Starkey, J. (1971) A refinement of the structure of anorthite. Zeitschrift für Kristallographie, 133:75-84.

Wenk, H.R., Joswig, W., Tagai, T., Korekawa, M., and Smith, B.K. (1980) Average structure of An 62-66 labradorite. American Mineralogist, 65, 81-95.

Wenk, H.R., and Nakajima, Y. (1980) Structure, formation, and decomposition of APBs in calcic plagioclase. Physics and Chemistry of Minerals 6, 169-186.

Xu, H., Shen, Z., Konishi, H., Fu, P., and Szlufarska, I. (2014) Crystal structures of laihunite and intermediate phases between laihunite-1M and fayalite: Z-contrast imaging and ab initio study. American Mineralogist, 99, 881-889.

Yamamoto, A., (1982) Structure factor of modulated crystal-structures. Acta Crystallographica, Section A 38, 87-92.

Yamamoto, A., Nakazawa, H., Kitamura, and M., Morimoto, N. (1984) The modulated structure of intermediate plagioclase feldspar $Ca_xNa_{1-x}Al_{1+x}Si_{3-x}O_8$. Acta Crystallographica, Section B 40, 228-237.

This is a preprint, the final version is subject to change, of the American Mineralogist (MSA)
Cite as Authors (Year) Title. American Mineralogist, in press.
(DOI will not work until issue is live.) DOI: http://dx.doi.org/10.2138/am-2015-5022 9/10

Figures captions

Figure 1: SAED pattern along ***a***-axis (A), Fast Fourier transform (FFT) patterns of annular bright-field (ABF) image (B), and Z-contrast image (C) of modulated bytownite. Satellite reflections do not occur around the 000 spot of FFT pattern (C).

Figure 2: ABF STEM image (A) image and Z-contrast image (B) along ***a***-axis. Arrows indicate ordering of Ca atoms (bright spots) at the boundary positions between the lamellae domains.

Figure 3: Noise-filtered Z-contrast image clearly showing Ca-Na ordering in lamellae domains and at the inversion boundary positions. Neighboring lamellae domains with $I1$symmetry are in inversion twin relationship. A unit cell structure model showing polarity of Na-Ca atoms is also overlaid on the image.

Figure 4: (A) Structure model for plagioclase with $C\bar{1}$ symmetry, i.e., average subcell structure of plagioclase. (B) Structure model ($I\bar{1}$) for the boundary between lamellae domains. (C) Structure model for the subcell ($I1$) of lamellae domain. (D) Structure model for the subcell that is in inversion twin relationship with (C). Neighboring lamellae domains are in enantiomorphic pairs, i.e., left-handed and right-handed structures. Oxygen atoms are omitted to enhance the structural differences.

Big yellow spheres: Ca; small yellow spheres: Na; blue spheres: Si: turquoise spheres: Al.

Figure 5: Projections of low-albite ($C\bar{1}$), anorthite ($I\bar{1}$), and anorthite ($P\bar{1}$) structures along their ***a***-axes showing positions of Na and Ca atoms in the structures. Oxygen atoms are omitted to enhance the structural differences.

Big yellow spheres: Ca; small yellow spheres: Na; Blue spheres: Si; turquoise spheres: Al.

Figure 6: Proposed model for modulated structure showing inversion boundaries // $(0\bar{1}1)$. Arrows indicate the boundaries. The boundary between neighboring lamellae domains has $I\bar{1}$ symmetry instead of $C\bar{1}$ symmetry. The periodicity in this figure is shorter than the periodicity in the actual crystal. This simplification is necessary in order to save page space.

Big yellow spheres: Ca; small yellow spheres: Na; blue spheres: Si; turquoise spheres: Al, or Al-dominated sites.

Figure 7: SAED pattern (A) and FFT pattern (B) along $[\bar{1}\bar{1}\bar{1}]$-zone-axis showing satellite reflections along ~ $(01\bar{1})$* direction.

Figure 8: Z-contrast image (A) and noise-filtered image (B) along $[\bar{1}\bar{1}\bar{1}]$-zone-axis showing modulation along ~ $(\bar{1}\bar{1}\bar{1})$* direction. Boundaries between neighboring lamellae domains are illustrated by yellow lines. A structural projection of $I1$ intermediate plagioclase (C) and a zoomed-in image (D) of sub-figure (B) show structural polarity with periodic big dark (D) and small less dark (LD) areas along ***c***-axis in the subcells of a lamellar domain. The polarity is a result of Ca-Na ordering (C).

Fig. 1

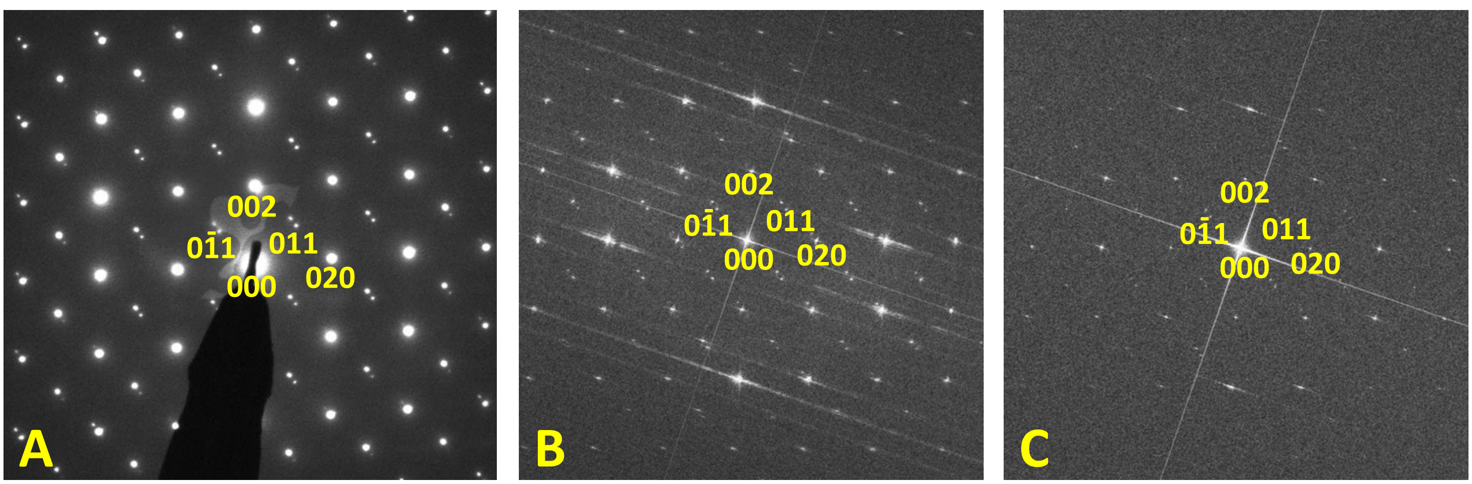

002
0$\bar{1}$1
011
000
020
A
002
0$\bar{1}$1
011
000
020
B
002
0$\bar{1}$1
011
000
020
C

Fig. 2

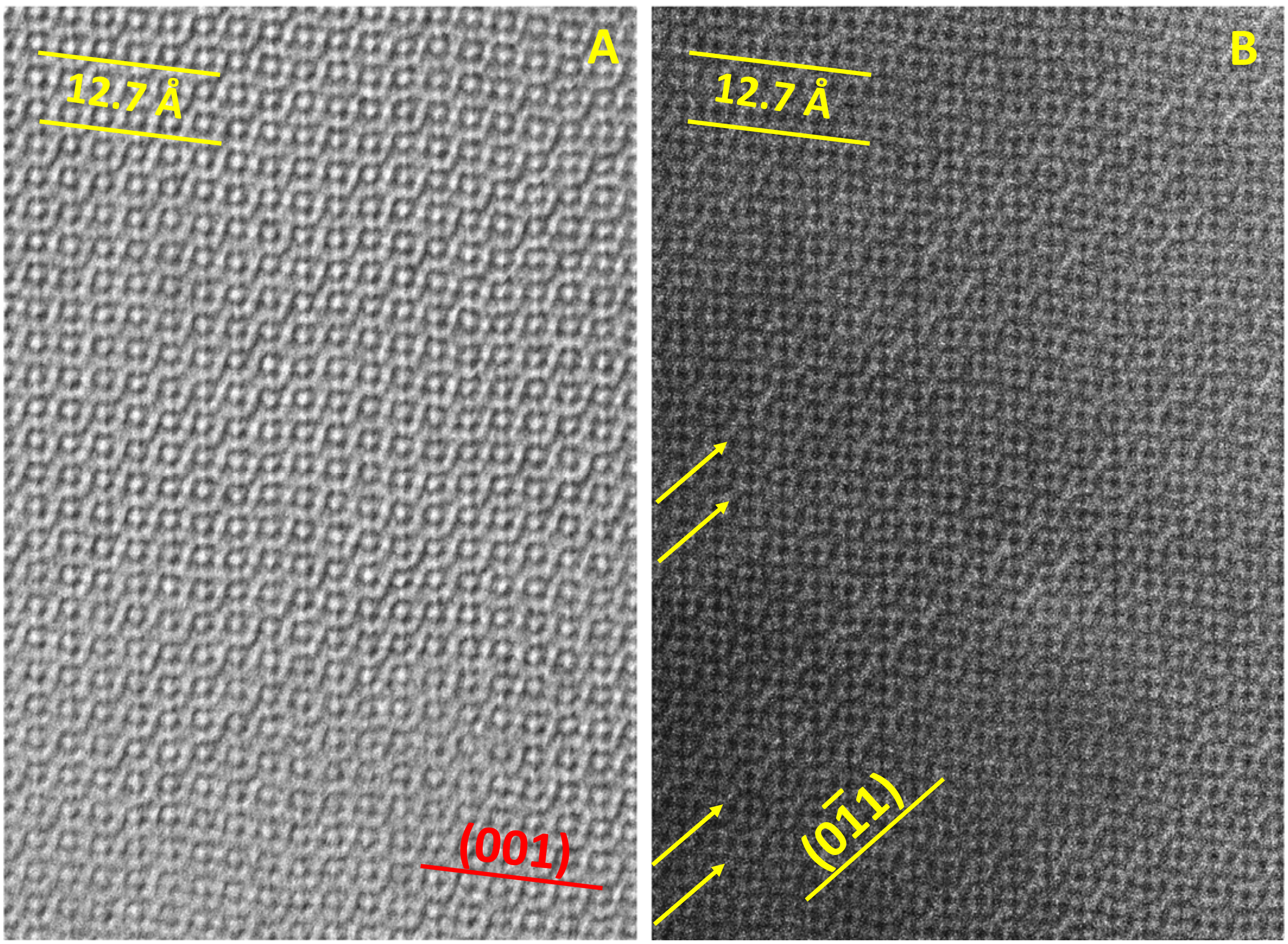

Fig. 3:

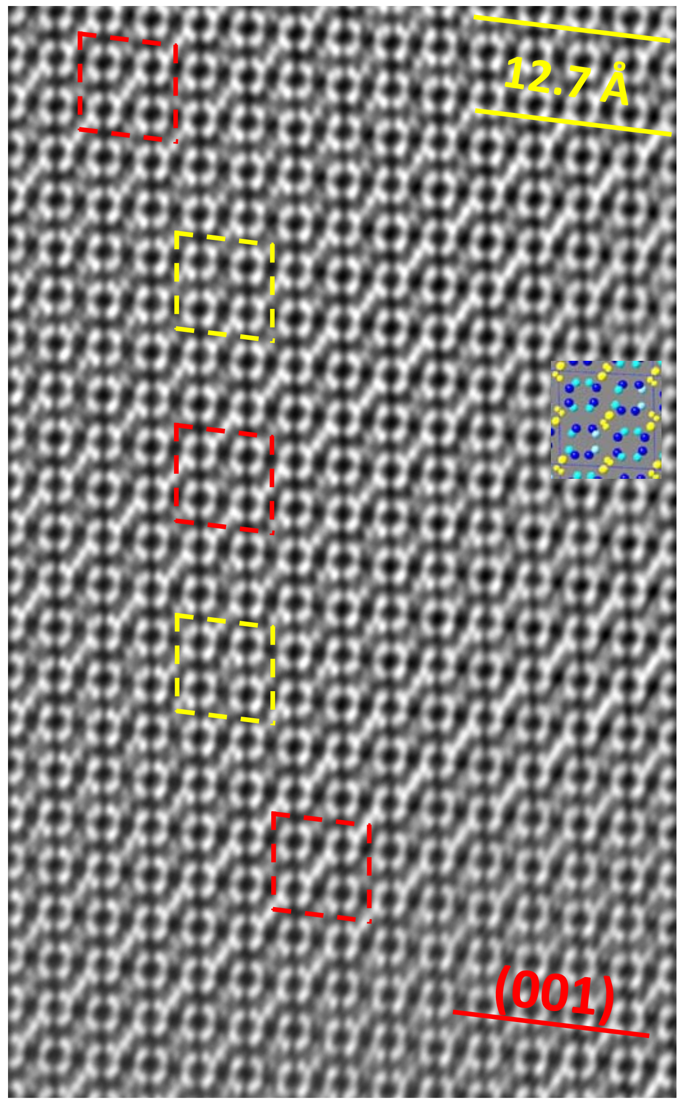

Fig. 4

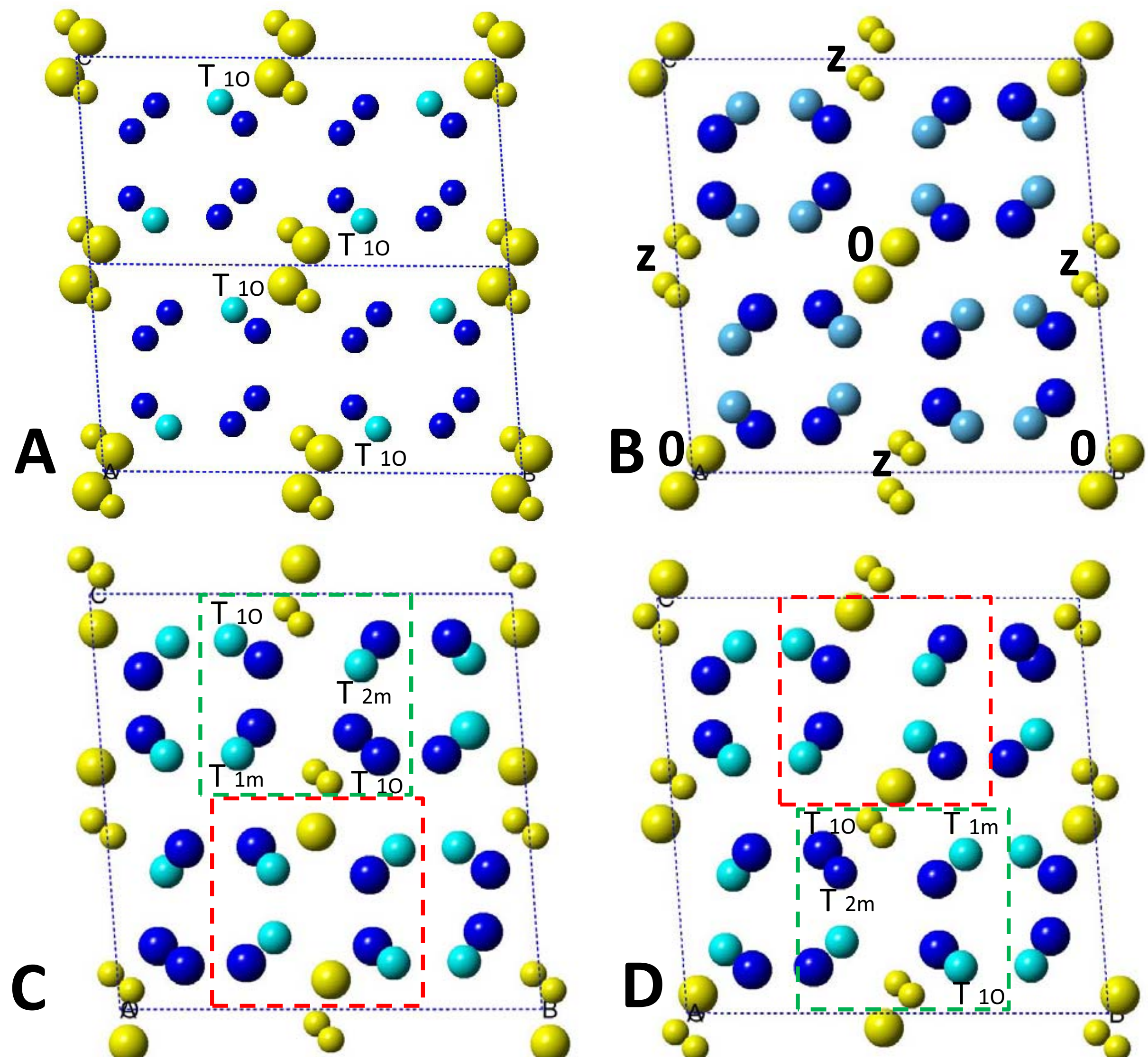

Fig. 5

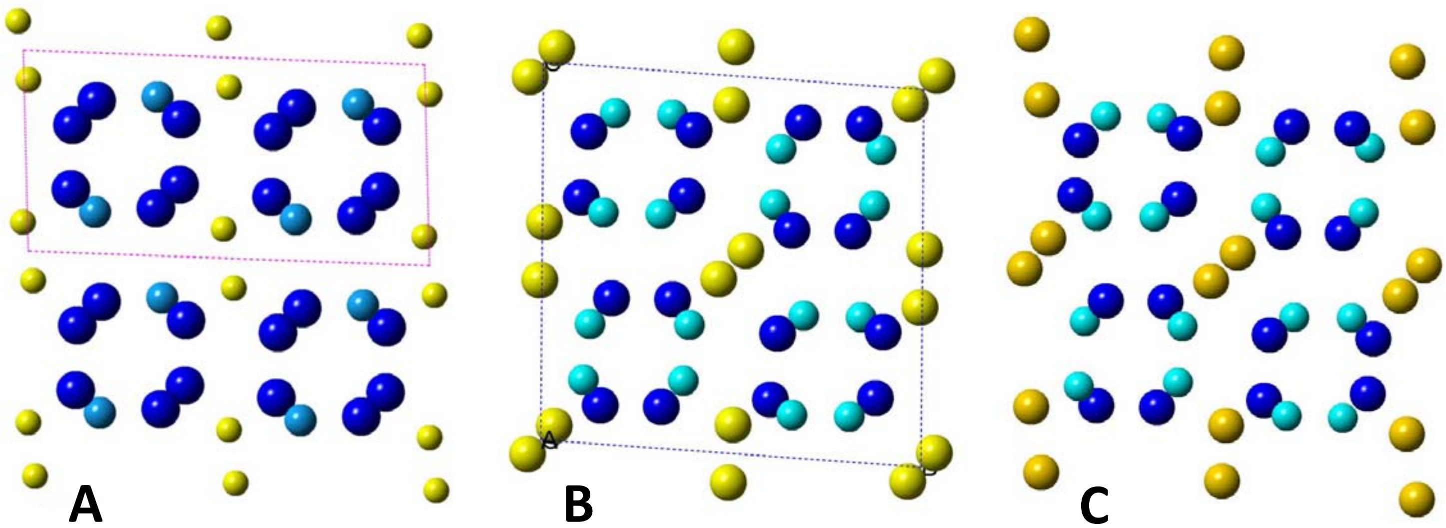

Fig. 6

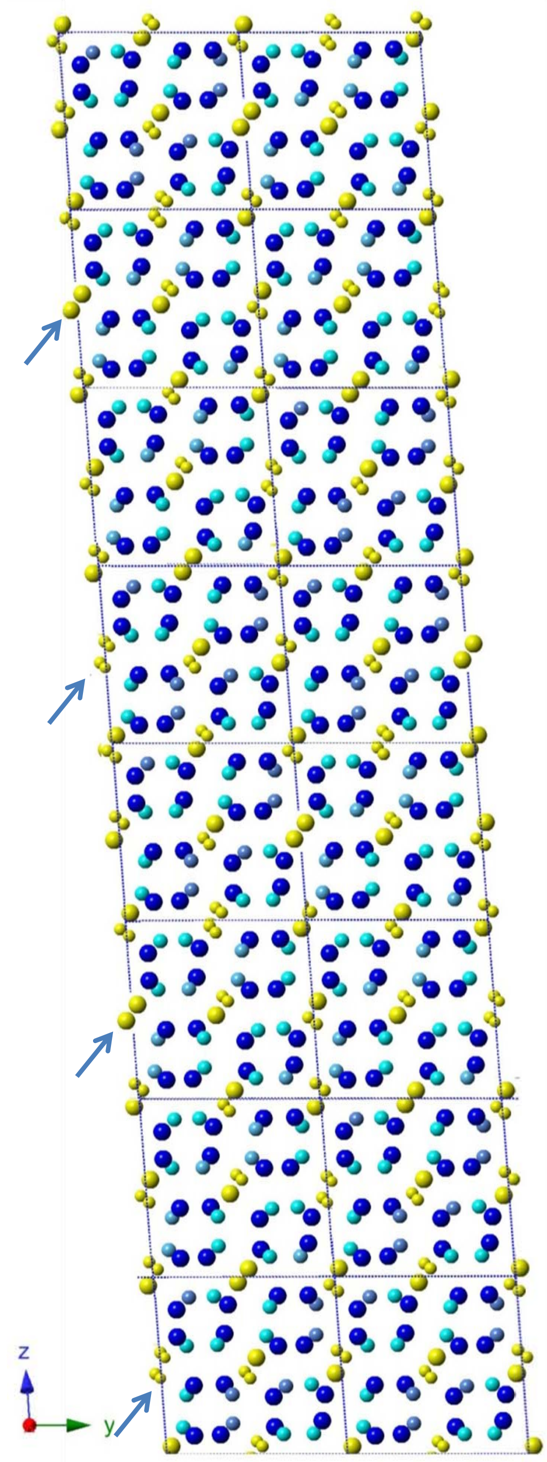

Fig. 7

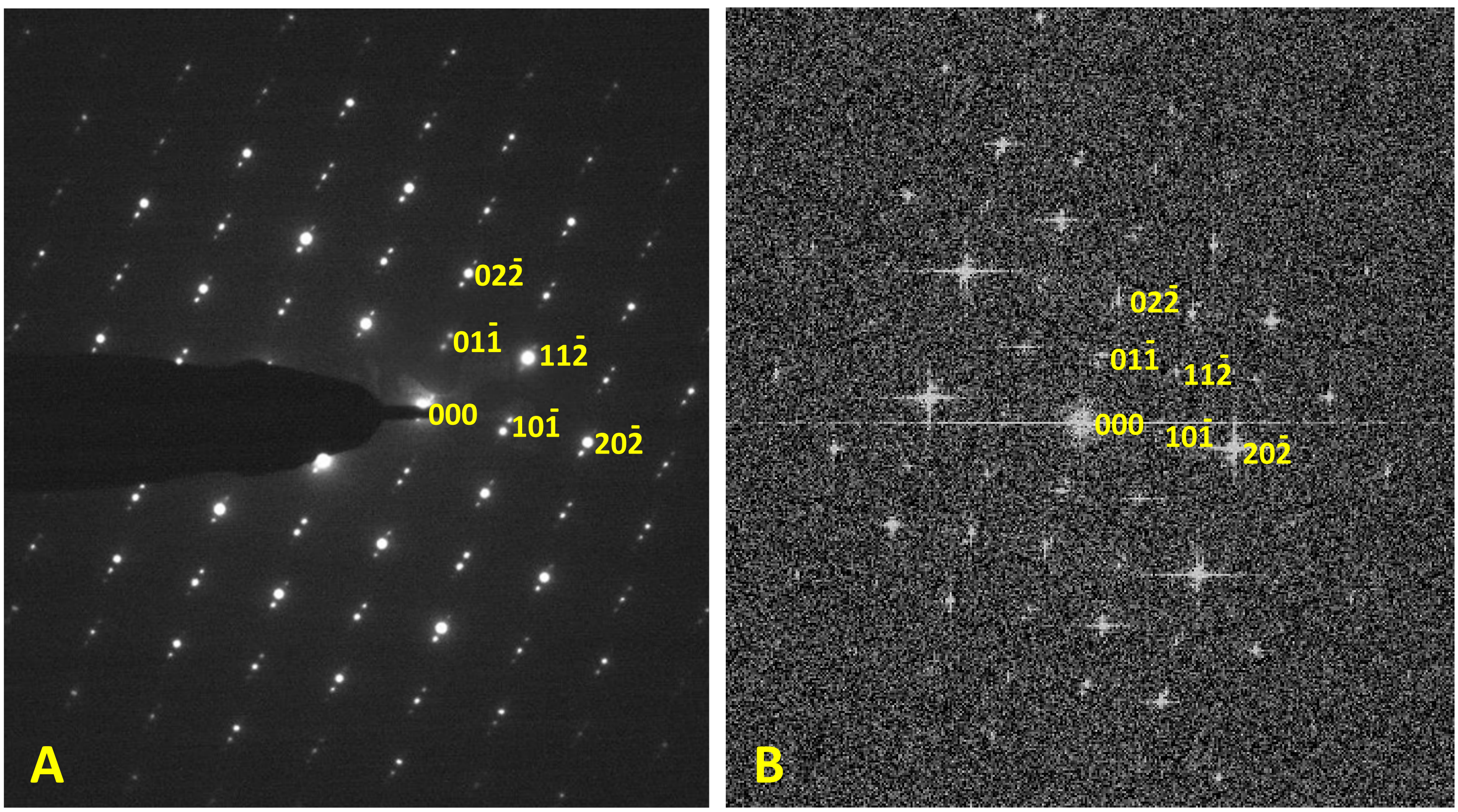
02$\bar{2}$
01$\bar{1}$
11$\bar{2}$
000
10$\bar{1}$
20$\bar{2}$
A
02$\bar{2}$
01$\bar{1}$
11$\bar{2}$
000
10$\bar{1}$
20$\bar{2}$
B

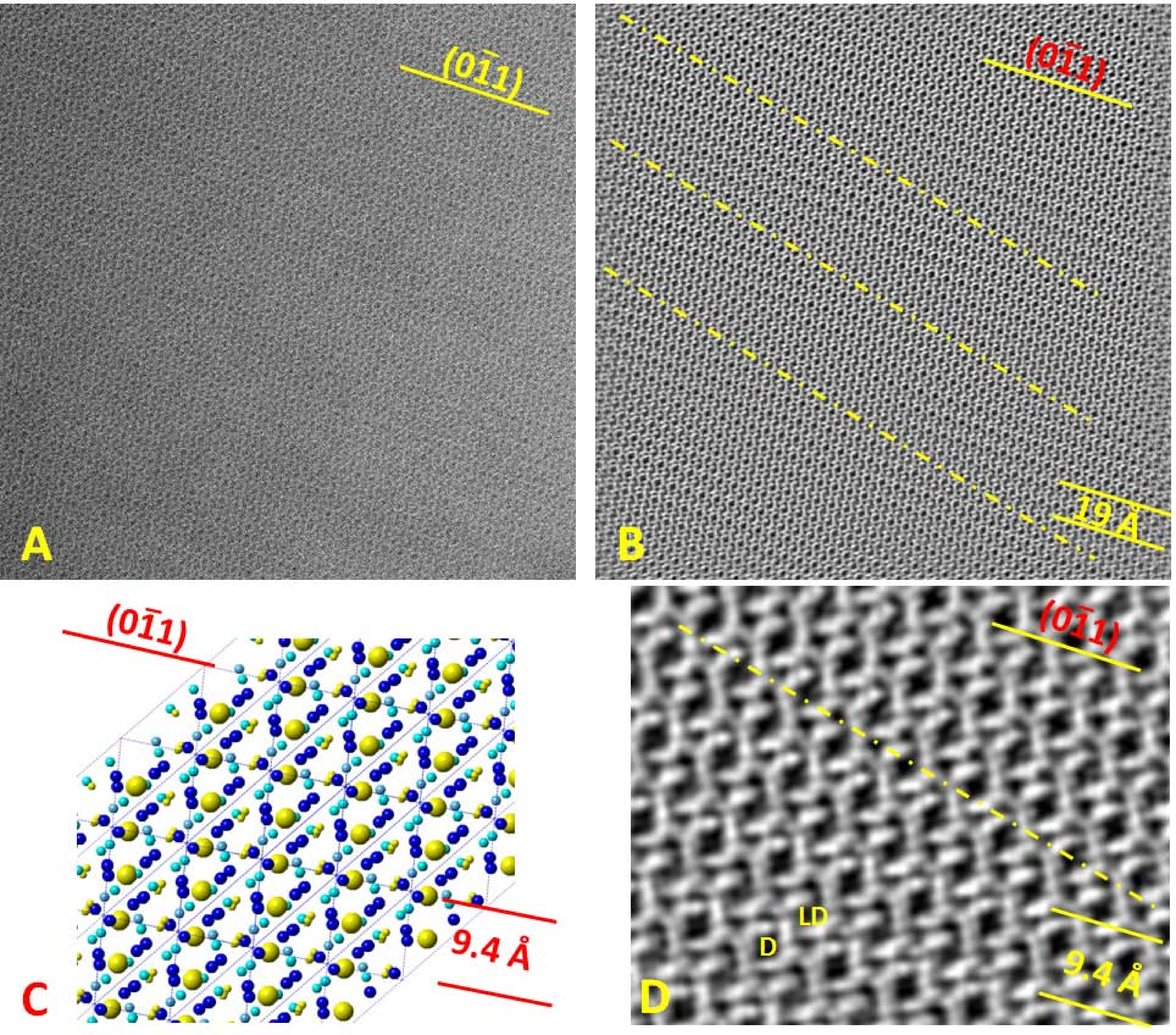

(0$\bar{1}$1)
A
(0$\bar{1}$1)
19 Å
B
(0$\bar{1}$1)
9.4 Å
C
(0$\bar{1}$1)
LD
D
9.4 Å
D